Phase change memory: Rationalizing the dominance of Ge/Sb/Te alloys

R. O. Jones
Peter Grünberg Institut PGI-1 and JARA/HPC,
*Forschungszentrum Jülich, D-52425 Jülich, Germany**
(Dated: January 6, 2020)

Rewritable optical storage is dominated by alloys of a small number of elements, overwhelmingly Ge, Sb, and Te. For over 30 years, Ge/Sb/Te alloys in the composition range $(GeTe)_{1-x}(Sb_2Te_3)_x$ ($0 \leq x \leq 1$) have been the materials of choice in commercial devices: all have metastable rock salt structures that change little over decades at archival temperatures, and all contain vacancies (cavities). The special status of Ge/Sb/Te alloys arises from the close similarity of their valence orbitals, as measured by the orbital radial moments, so that bonds are stronger than in other combinations of elements of groups 14–16 with appropriate valences. The orbital similarity arises from the irregular changes in atomic orbitals and properties as the atomic number increases ("secondary periodicity"). H. Jones showed (1934) that the simple cubic structure of (metallic) Bi (valence configuration $6s^26p^3$) is unstable to a distortion to a (semimetallic) rhombohedral structure. This picture can be adapted to Ge/Sb/Te alloys to explain the metastable structure of the above family of compounds, where vacancies almost always occur next to Te atoms, which form one sublattice of the rock salt structure. The disorder in the Ge/Sb/vacancy sublattice is not random.

I. INTRODUCTION

Phase change materials (PCM) dominate the world of rewritable optical storage media, including the digital versatile disk (DVD-RW) and the Blu-ray Disc (BD-RE), and are leading candidates for future non-volatile computer memories, such as PC-RAM. Nanosized bits in a thin polycrystalline layer are switched reversibly and extremely rapidly between amorphous (*a*-) and crystalline (*c*-) states, which can be identified by measuring the resistivity or optical reflectivity. Ovshinsky [1] showed that this process could be induced by an electric field in materials containing elements of groups 13 – 16, particularly Te and As, and the search for materials that crystallize rapidly at high temperatures while retaining data for many years at room temperature has focused on narrow gap semiconductors (NGS) containing these elements. Compounds containing Te [2] and Sb have always been favorites: amorphous Te films crystallize spontaneously above 0°C, and *a*-Sb likewise at higher temperatures, so that these elements must be stabilized against premature crystallization by added components. The identification of materials with satisfactory properties for crystallization *and* amorphization proved to be difficult.

Chen *et al.* [3] showed that laser-induced crystallization occurred in films of Te in 100 ns and in GeTe [to the face-centered cubic (FCC) form] in less than 30 ns, with good data retention. $Te_{1-x}Ge_x$ films and the stoichiometric compounds Sb_2Se_3, Sb_2Se, and Sb_2Te_3 could be crystallized with laser pulses of less than 1 μs, but GeSe and $GeSe_2$ required much longer crystallization times. Popular compounds containing Te include Sb/Te alloys near the eutectic composition $Sb_{0.7}Te_{0.3}$, with small amounts of other elements (Ag, In in AIST, Ge in GeST), and the pseudobinary materials $(GeTe)_{1-x}(Sb_2Te_3)_x$ [4]. The phase diagrams of $Ge_2Sb_2Te_5$ (GST, x=1/3), $Ge_1Sb_2Te_4$ (x=1/2), and $GeSb_4Te_7$ (x=2/3) [5], related Ge/Bi/Te compounds [6], and other homologs [7] have been determined. The crystalline structures comprise layers, up to 66 in the unit cell of $GeSb_8Te_{13}$ (x=4/5). Recent years have seen focus on compounds containing indium and Ge, Sb, and Te, including $InGeTe_2$ [8], In_3SbTe_2 [9–11], and In_2GeTe_3 [11]. These compounds often share the rock salt structure of Ge/Sb/Te compounds.

Yamada [12, 13] reviewed the development of PCM using Ge/Sb/Te alloys, particularly those in the above family, and noted that they provided "the first practical phase change materials and still today (2012) remain the standard material" [14]. The crystalline (rock salt, RS, $Fm\bar{3}m$) phases show wide composition tolerance and are metastable over many years at archival temperatures, and the amorphous forms resist crystallization at room temperature. The structure of the metastable form, particularly the presence of vacancies (cavities) is crucial. Yamada [15] proposed that sites of the anion sublattice were occupied by Te atoms, and the cation sublattice randomly by Ge and Sb atoms and vacancies.

X-ray diffraction measurements on 17 alloys [16] showed that the fraction of vacancies in the cation sublattice varies approximately as $x/(1 + 2x)$ (20% for GST). Annealing of the metastable structures at sufficiently high temperatures results in more stable layered structures (trigonal [5]) that comprise, in the case of GST, stacks of nine layers (-Te-Sb-Te-Ge-Te-Ge-Te-Sb-Te-) separated by a gap [17] arising from the ordering of vacancies. The analysis of Matsunaga *et al.* [18] showed mixed Sb-Ge layers, with "Sb" and "Ge" being replaced by "Sb-rich" and "Ge-rich," respectively. Recent scanning tunneling electron microscopy (STEM) measurements [19] on GST show that different annealing

* Electronic mail: r.jones@fz-juelich.de

conditions lead to different occupations of Ge and Sb in the cation planes, with Sb enrichment in the planes closest to the gaps, and to different distributions of stacking sequences of 7, 9, and 11 planes.

There have been countless studies of phase change properties in alloys of elements of groups 13–16, particularly those near the diagonal in the periodic table between B and Po. A few such elements—particularly Ge, Sb, and Te—have dominated practical PCM applications. Work on optical memory has focused on "GeTe-rich" materials, such as the Blu-ray Disc material $Ge_8Sb_2Te_{11}$ (x=1/9) [20], and recent developments also involve these elements. Research on "superlattices" with much improved power requirements has focused on alternating nanoscale layers of GeTe and Sb_2Te_3 in thin films [19, 21, and references therein]. Crystallization speedup was obtained by improving the thermal stability of a-Sb_2Te_3 by alloying with scandium ($Sc_{0.2}Sb_2Te_3$, [22]), and by confining Sb samples to extremely small volumes [23]. Why have these elements, particularly Ge/Sb/Te alloys near the GeTe-Sb_2Te_3 tie-line, dominated the discussion?

Coordinate schemes have proven to be valuable in distinguishing between structural types in binary NGS [24] and PCM [25] and are discussed in Sec. II. We calculate and discuss the valence orbitals and related properties in Ge, Sb, Te and other atoms in groups 13–16, and show that the orbitals vary irregularly with changing atomic number ("secondary periodicity"). In Sec. III, we discuss the structural instabilities associated with partially occupied nearly free electron (NFE) bands and the role played by the average number of valence electrons. In Sec. IV we summarize experimental information and simulations concerning crystallization of a-GST [26–30], also from the perspective of Ostwald's step rule, where multistage processes can aid the transition from the metastable liquid to the most stable (trigonal) structure. We discuss the results and summarize our findings in Sec. V. Bonding concepts in these and other materials have been reviewed elsewhere [31].

II. STRUCTURES, COORDINATE SCHEMES, VALENCE ATOMIC ORBITALS

A. Coordinate schemes

Trends in structures and other properties of elements and compounds can often be clarified if plotted with appropriate variables (coordinates), examples being the the rows and columns of the periodic table. Elements to the left are metals, while most others are covalently bonded semiconductors and insulators, with a tendency to metallic behavior as the atomic number Z increases. The group 14 elements, for example, change with increasing Z from insulating diamond through semiconducting Si and Ge to metallic forms of Sn and Pb. Pauling [32] discussed the properties of atoms in terms of their location in the periodic table and defined their electronegativities in terms of bond energies of small molecules. Mulliken [33] defined electronegativity in purely *atomic* terms as the average of ionization energy and electron affinity. The present work follows the latter in focusing on the constituent atoms.

Discussions of structures of binary (AB) compounds often focus on the differences between the coordinates of A and B. Phillips and van Vechten [34] used the ionic and covalent contributions to the average gap in octet compounds A^NB^{8-N}, and St. John and Bloch [35] plotted differences in electronegativity (or ionicity) against the average hybridization in these materials. Both schemes could differentiate between structures with different coordination numbers, and Schiferl [36] used a similar approach to study A^NB^{10-N} compounds with average valence five, denoted $\langle \mathbf{5} \rangle$ below.

Coordinate plots can be made using distances corresponding to the maxima of valence orbital functions for an atomic model potential [35], the crossing points of atomic pseudopotentials [37] or their valence orbitals [38]. Littlewood [39] showed that more ionic 14-16 compounds have the RS structure, while less polar bonding leads to rhombohedral structures and large covalent gaps to the orthorhombic structure. These coordinate schemes were reviewed by Littlewood [24], who studied structural types in many NGS with octet and A^NB^{10-N} compositions, many of which show only small deviations from perfect sixfold or eightfold coordination.

PCM often comprise three or even four elements, but schemes for binary compounds can be adapted by replacing the multielement compound by an equivalent binary material. For example, Ge and Sb atoms in crystalline Ge/Sb/Te-materials occupy one sublattice of an RS structure, and a stoichiometrically averaged coordinate can be derived [25]. PCM materials with favorable properties are generally found in the region with small ionicity and weak hybridization. This picture can be extended using the coordinates of electrons shared and transferred between domains surrounding the individual nuclei, with a third coordinate for particular physical properties [40].

B. Atomic orbitals, density functional calculations

Valence atomic orbitals determine the "size" and electronegativity of an atom, and the relationships between orbital overlap, hybridization, and bond strength go back to the early days of the quantum theory of molecules [32, 41, 42]. The bond strength, in particular, is largest if the orbital overlap is a maximum. We focus here on trends in the s- and p-valence orbitals in groups 13–16 elements obtained from density functional (DF) calculations [43] using the Perdew-Burke-Ernzerhof (PBE) [44] approximation to the exchange-correlation energy. The all-electron (semi-relativistic) calculations were carried out using a modified form of the program of Hamann [45]. The atomiclike mass-velocity and Darwin terms are

treated explicitly, and spin-orbit coupling effects are included by perturbation theory [46].

C. Orbital trends and secondary periodicity

Biron noted over 100 years ago [47] that many chemical and physical properties exhibited "secondary periodicity," a zigzag behavior superimposed on a smooth trend down a column of the periodic table. He showed that this complicates the prediction of properties by interpolation, examples being the heats of formation of oxides and chlorides of groups 15, 16, and 17 and the fact that the group 15 elements P and Sb are pentavalent, while N, As, and Bi are trivalent. Anomalously large ionization energies are evident in fourth row compounds [48] and in the s-d excitation energies and the s^2-s^1 ionization energies in group 15 ions [49]. Secondary periodicity [48, 50] is associated with the stronger and shorter bonds that are consequences of the incomplete screening by the $3d$-electrons of the additional nuclear change in elements beyond Ga (Z=31, "d-block contraction") and by the $4f$-shell in elements beyond Tl (Z=81). The latter effect had been observed in 1925 in crystallographic measurements of oxides and termed "lanthanide contraction" [51].

Most PCM comprise elements of groups 13–16, and almost all are near the diagonal in the periodic table between B and Po. The valence orbitals of group 14 elements are shown in Fig. 1 and those of groups 13, 15, and 16 in Fig. SF1–3 of the Supplementary Material [52]. The p-orbitals in Si and Ge are strikingly similar and differ from those of Sn and Pb, which are again very similar. Pairwise similarity is a reflection of secondary periodicity and is evident in all four groups. The trends can be quantified in several ways, including the energy eigenvalues ε_{nl}, where eigenvalue splitting between the s- and p-valence orbitals is one measure of the tendency of the atomic orbitals to form sp-hybrids and directed bonds [24]. These eigenvalues are given for groups 13–16 in Table I and Fig. SF4 [52], but their interpretation requires care. The splitting in C, for example, is *larger* than in Si, Ge, or Sn, although sp-hybridization is strongest in C. The radii of the maxima in these orbitals or those derived from an atomic model potential have also been used [25, 35, 39].

We focus here on the first radial moment of the orbitals or the normalized expectation value of r with respect to the orbitals

$$\langle r\rangle_{nl} = \int dr\ r\ |rR_{nl}|^2 \Big/ \int dr\ |rR_{nl}|^2\ , \qquad (1)$$

which probes an orbital over its entire range, including the tail. The results are provided in Fig. 2 and Table I. For Ge, Sb, and Te the values of $\langle r\rangle_{nl}$ are 20–30 % greater than the radii where $R_{nl}(r)$ is a maximum [53]. Orbital comparisons weighted towards small values of r are provided by $\langle r^{-1}\rangle_{nl}$, which is defined analogously and is sometimes used in the generation of pseudopotentials. Values of this moment are given in Table I for completeness.

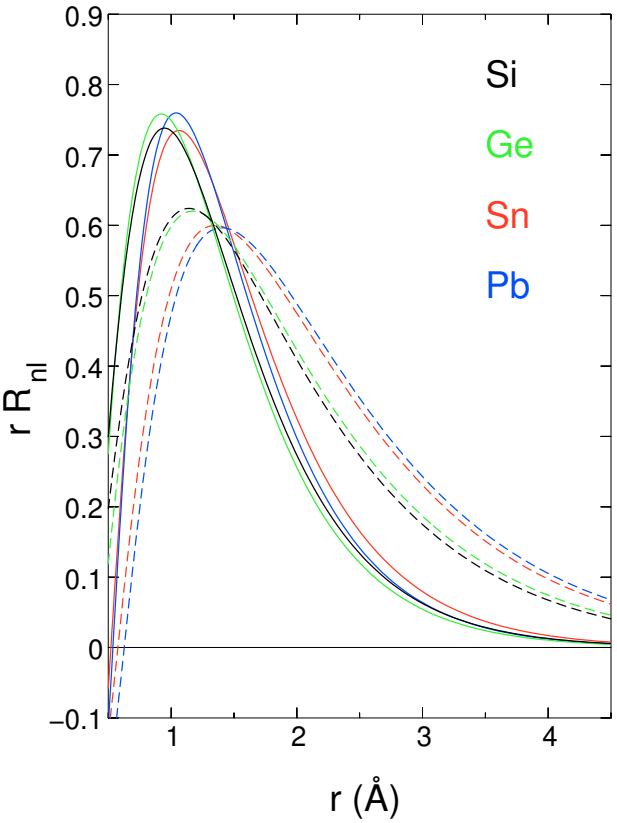

FIG. 1. Radial orbital functions rR_{nl} ($n = 2-6$) for s- (solid curves) and p- (dashed curves) valence electrons in group 14 elements. Secondary periodicity is particularly evident in the p-orbitals.

The first radial moment provides a consistent picture of trends of atoms in these groups, and secondary periodicity is most pronounced in group 13 elements and more evident in s-orbitals than in p-orbitals. The structural consequences are immediate. The contraction of the $4s$ and $4p$-orbitals in Ga is so large that they are more compact than the $3s$ and $3p$-orbitals in Al (Fig. SF1 [52]), and the $^3\Sigma_u^-$ state is *shorter* in the dimer Ga_2 than in Al_2 [54]. The $3p$-orbital in Si and the $4p$-orbital in Ge (and the positions of their maxima) are very similar, and the $4s$-orbital in Ge is even more compact than the $3s$-orbital in Si. The secondary periodicity evident in the orbitals and moments in group 14 elements is consistent with the trend in the measured lattice constants with the diamond structure (C: 3.567 Å, Si: 5.431 Å, Ge: 5.646 Å, grey Sn: 6.489 Å) and other properties.

The maxima in the $2s$-and $2p$-functions (Fig. SF5) and the corresponding moments (Table I) are similar in all first row elements, where there are no core p-electrons to reduce the interaction of the $2p$-electrons with the nucleus, and sp-hybridization is stronger. This results in C in stronger and more flexible (single, double, and

TABLE I. Moments $\langle r\rangle_0$ and $\langle r\rangle_1$ (Å) and $\langle r^{-1}\rangle_0$ and $\langle r^{-1}\rangle_1$ (Å^{-1}), and the corresponding DF eigenvalues ε_0 and ε_1 (hartree) for s- and p valence orbitals of atoms of groups 13, 14, 15, and 16.

Group	Element	$\langle r\rangle_0$	$\langle r\rangle_1$	$\langle r^{-1}\rangle_0$	$\langle r^{-1}\rangle_1$	ε_0	ε_1
	B	1.033	1.218	1.390	1.125	-0.347	-0.133
	Al	1.346	1.824	1.000	0.735	-0.285	-0.100
13	Ga	1.240	1.812	1.055	0.725	-0.329	-0.095
	In	1.381	1.980	0.931	0.649	-0.302	-0.093
	Tl	1.311	2.039	0.973	0.627	-0.351	-0.087
	C	0.832	0.953	1.740	1.451	-0.506	-0.194
	Si	1.145	1.479	1.186	0.914	-0.398	-0.150
14	Ge	1.120	1.534	1.172	0.855	-0.431	-0.143
	Sn	1.265	1.728	1.021	0.745	-0.385	-0.132
	Pb	1.223	1.787	1.046	0.711	-0.443	-0.129
	N	0.698	0.786	2.083	1.772	-0.686	-0.264
	P	1.003	1.256	1.363	1.084	-0.514	-0.203
15	As	1.026	1.352	1.284	0.972	-0.533	-0.191
	Sb	1.178	1.545	1.098	0.832	-0.472	-0.178
	Bi	1.150	1.619	1.116	0.785	-0.532	-0.168
	O	0.603	0.670	2.423	2.089	-0.881	-0.332
	S	0.897	1.096	1.535	1.247	-0.634	-0.258
16	Se	0.950	1.219	1.393	1.083	-0.635	-0.240
	Te	1.104	1.414	1.177	0.912	-0.553	-0.219
	Po	1.088	1.494	1.184	0.852	-0.622	-0.207

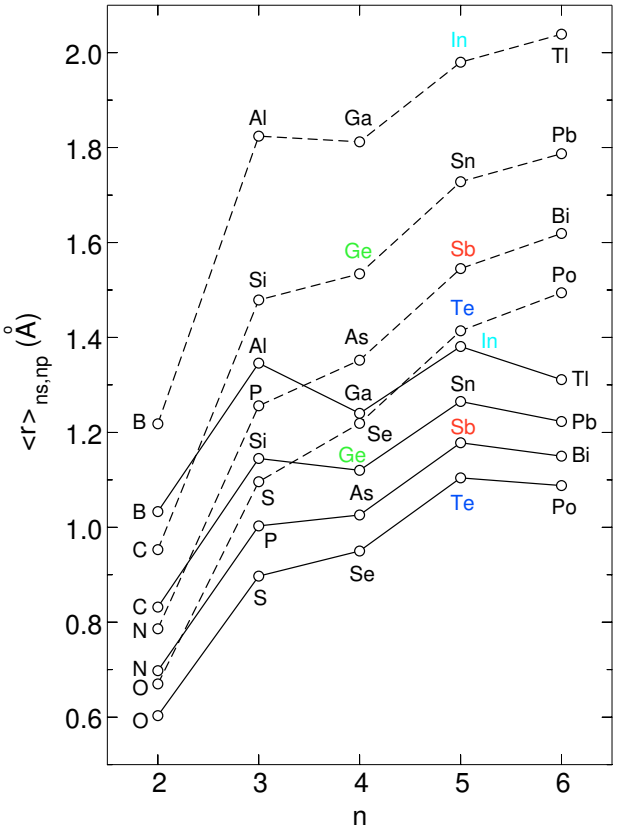

FIG. 2. First radial moments (Eq. 1) for s- (solid curves) and p- (dashed curves) valence electrons in elements of groups 13–16.

triple) bonds than in other group 14 elements, where the p-functions are significantly more diffuse than the s-functions, and single bonds are favored [55]. Relativistic effects [50] in elements with $Z > 81$ lead to contraction of the orbitals of the innermost electrons and by orthogonalization to more compact s-valence orbitals, with lower energy eigenvalues and weaker sp-hybridization. This is reflected in the cubic structures of PbS, PbSe, and PbTe.

The valence orbital functions for Ge, Sb, and Te (Fig. 3) are remarkably similar for elements with a large range of Z: 32 (Ge) to 52 (Te). Orbitals become more compact on moving from left to right in the periodic table, counteracting the tendency to more extensive orbitals as the row number or principal quantum number increases. The radial moments give a direct measure of the electronegativity of the elements, and we note that the Pauling electronegativities are almost identical in Ge (2.01), Sb (2.05), and Te (2.1) [56]. Also shown as Supplementary Material are the valence orbitals of the first-row elements B–F (Fig. SF5 [52]) and the component elements of AIST (Ag, In, Sb, Te) and Ge (Fig. SF6).

III. STRUCTURAL CHANGES IN GST - INGREDIENTS OF A MODEL

The most stable (trigonal) structures of Ge/Sb/Te alloys have never been used in commercial PCM, and the metastable rock salt structure is viewed as the "key" to their superior phase change properties [14]. Particularly important are the wide range of compositions covered by the tie line and that small departures from this line also lead to cubic structures.

Vacancies in GST are structural features, not defects [57], and their number maximizes the occupation of bonding p-orbitals [25, 58], whose overlap is greatest for bond angles near 90° [41]. Cubic structures are often favored in such cases, although the crystal structures in Sb and P [59] and related clusters [60–62] suggest treating this assumption with care [63]. DF calculations indicated that cubic (p-bonding) structures are favored over chalcopyrite (sp^3-hybridized) structures in Te-based ternary PCM if the total occupancy of valence electrons $N_{sp} > 4.1$ [58]. We use the NFE approximation of Peierls [64] to discuss the structures of PCM and their distortions

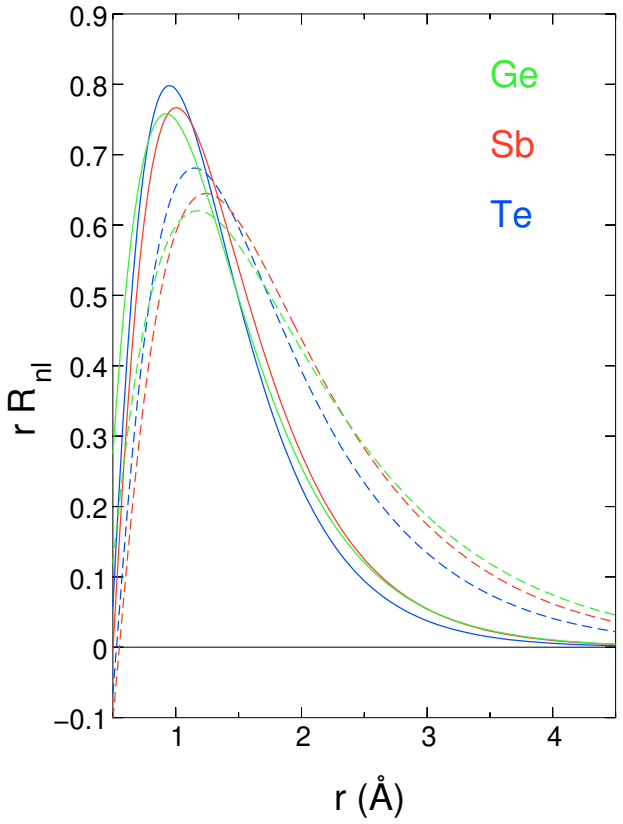

FIG. 3. Radial orbital functions rR_{nl} for s- (full curves) and p- (dashed curves) valence electrons in Ge (green), Sb (red), and Te (blue).

A. Nearly free electron (NFE) model

Bloch [65] showed that the eigenfunctions of an electron in a periodic potential $V(\mathbf{r})$ can be written

$$\psi_{\mathbf{k}}(\mathbf{r}) = u_{\mathbf{k}}(\mathbf{r}) \exp i(\mathbf{k}\cdot\mathbf{r}), \tag{2}$$

where $u_{\mathbf{k}}(\mathbf{r})$ has the periodicity of $V(\mathbf{r})$. If V vanishes [free-electron (FE) model], the eigenvalues are $E_{\mathbf{k}}(\mathbf{r}) = \hbar^2k^2/2m$, where $k = |\mathbf{k}|$. The reciprocal lattice points for a linear chain of periodicity a are the values in k-space where $\exp(ikx)$ has periodicity a, i.e. $g = n\pi/a$, where n is an integer. Peierls [64] showed that a gap in the band structure of $|2V_g|$ occurs at $k = g/2$ (Fig. 4), where V_g is the Fourier transform of V.

A periodic, three-dimensional potential $V(\mathbf{r})$ can be expanded as a Fourier series

$$V(\mathbf{r}) = \sum_{\mathbf{g}} V_{\mathbf{g}} \exp i(\mathbf{g}\cdot\mathbf{r}), \tag{3}$$

with

$$V_{\mathbf{g}} = \frac{1}{V}\int d\mathbf{r}\; V(\mathbf{r}) \exp -i(\mathbf{g}\cdot\mathbf{r}). \tag{4}$$

Brillouin [66] showed how to construct polyhedral zones in two and three dimensions using planes bisecting each

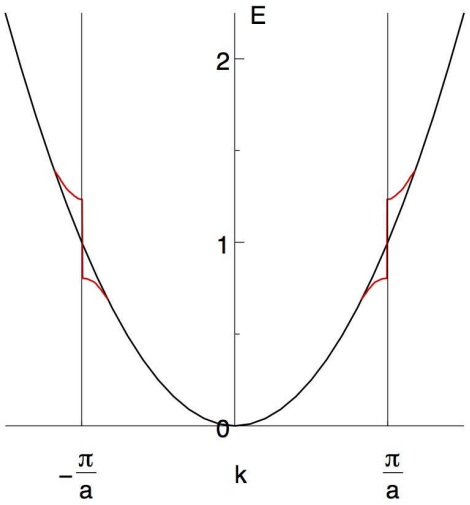

FIG. 4. Nearly free electron model of Peierls [64].

$\mathbf{g}$-vector, and the the smallest is the first Brillouin zone (BZ). Energy bands for larger values of $\mathbf{k}$ can be folded into this BZ to give the electronic band structure in the reduced zone scheme. If the structure has several atoms in the unit cell, $V_{\mathbf{g}}$ is replaced by $V_{\mathbf{g}}S_{\mathbf{g}}$, where the structure factor

$$S_{\mathbf{g}} = \sum_{\mathbf{r}_i} \exp -i(\mathbf{g}\cdot\mathbf{r}_i). \tag{5}$$

and $\mathbf{r}_i$ are the coordinates of the atoms in the unit cell of volume V [67]. $V_{\mathbf{g}}$ vanishes if $S_{\mathbf{g}}$ is zero, and the corresponding surfaces should not be counted as zone boundaries. This construction in the extended zone scheme was introduced by H. Jones [68], and we return to it below.

The FE and NFE models provide an excellent basis for studying metals and semiconductors. Mott and Jones [69, pp. 125-128] noted over 80 years ago that the conduction band widths measured in x-ray emission from many metals was close to the FE bandwidths calculated for the appropriate electron densities, and this is also true for many semiconductors. Figure 5 shows FE bands for structures with the translational symmetry of the FCC lattice (includes the diamond and RS structures), together with the degeneracies of the bands and the Fermi energy E_F if there are 8 (diamond) and 10 (RS) valence electrons in the unit cell. The large degeneracies of the bands near E_F in the latter suggest that a material with 10 valence electrons will have several bands near E_F derived from the FE bands along Λ and Q. The lower degeneracies and smaller value of E_F in the diamond structure imply fewer band crossings.

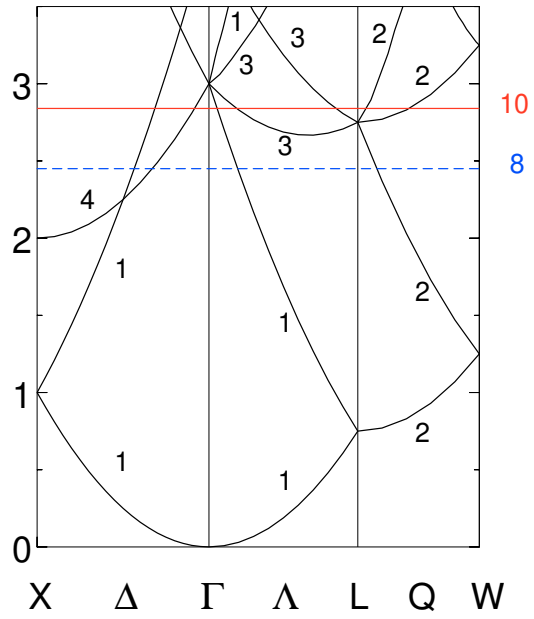

FIG. 5. Free-electron bands for structures with the translational periodicity of FCC lattices. X: 100, Γ: 000, L: $\frac{1}{2}\frac{1}{2}\frac{1}{2}$, W: $1\frac{1}{2}0$ [in units of $(2\pi/a)$, where a is the lattice constant]. Energies in units of $(2\pi/a)^2$. Also shown are the band degeneracies and the Fermi energies corresponding to 8 (blue, dashed) and 10 (red, solid) valence electrons in the unit cell.

B. Jones zones in extended k-space, "Peierls distortion"

A simple extension of the NFE model suggests a mechanism for structural distortions [70]. If we displace, for example, every second atom in a linear chain by the same amount, we double the size of the unit cell and can introduce gaps in the energy eigenvalue spectrum at half of the distance to the boundary of the original BZ ($\pm\pi/(2a)$) in Fig. 4. If this gap is at or near E_F, as in the case of a half-filled band, the distortion will be accompanied by a lower total energy. This mechanism in a 1D-system is often referred to as the "Peierls distortion" [70], but it was applied much earlier by H. Jones to the 3D-structure and electronic properties of the semimetal Bi [68, 69, 71] and other materials.

If there are two or more electrons in the unit cell, the first band (and BZ) are occupied, and it is convenient to discuss the bands near E_F using the *extended* zone scheme. The group 15 elements As, Sb, and Bi have five valence electrons per atom and are metallic in the SC structure, which can be represented (Fig. 6) as two FCC lattices displaced by half of the body diagonal. Two independent distortions, a relative displacement u of the FCC lattices and a trigonal shear (angle α) along the diagonal lead to the $A7$ (rhombohedral) structure found in these three elements [72]. The RS and rhombohedral structures of GeTe are related in the same way. In this picture, the $A7$ structure of Bi is simply a consequence of the instability inherent in a SC structure with half-filled bands. The distortion, which decreases in the order As→Sb→Bi as *sp*-hybridization weakens, yields a structure with short and long bonds that can be associated with the softening of the transverse optical (TO) phonon in the (111) direction.

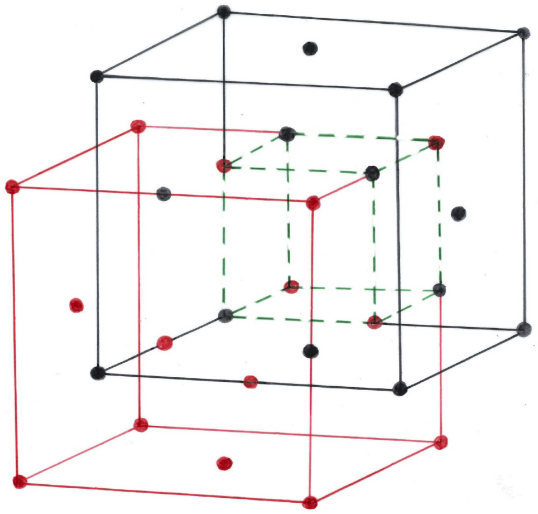

FIG. 6. SC structure (green, dashed) represented as two FCC lattices (red, black) displaced by half of the body diagonal of the latter.

The structures of As, Sb, Bi, and GeTe have two atoms and 10 valence electrons in the unit cell, so that at least five BZ are occupied. The fifth BZ has a complex form [Fig. 7(c)], and Jones adopted an alternative zone bounded by planes corresponding to large values of $S_{\mathbf{g}}$. The "Jones zones" (JZ) for 10 electrons [trigonal, Fig. 7(d)] has six planes arising from reciprocal lattice vectors of the form $[1\bar{1}0]$ and six from vectors related to [221]. It is much simpler than the fifth BZ, but it has the same volume and contains five states per atom [73]. The small number of $V_{\mathbf{g}}$ and the presence of parallel zone faces give rise to pairs of bands that are nearly parallel in a significant volume of **k**-space and give rise to characteristic peaks and shoulders in the optical properties.

The calculations of Jones [68, 69] focus on the Landau-Peierls diamagnetism and consider neither Pauli paramagnetism nor spin-orbit coupling, but they explained the rhombohedral structure of Bi, which results in an overlap between valence and conduction bands. The electron and hole pockets in the Fermi surface are consistent with the high diamagnetism and low (semimetallic) conductivity of Bi, and this applies also to As and Sb, and to GeTe, where the rhombohedral form is a narrow-gap semiconductor. The form of the FE bands near E_F suggests that valence band occupancies close to 10 will also have overlapping bands and similar (semimetallic) properties.

The Jones zone construction also provides insight into the electronic structure and optical properties of the semiconductors Si and Ge [31, 74]. The JZ for the di-

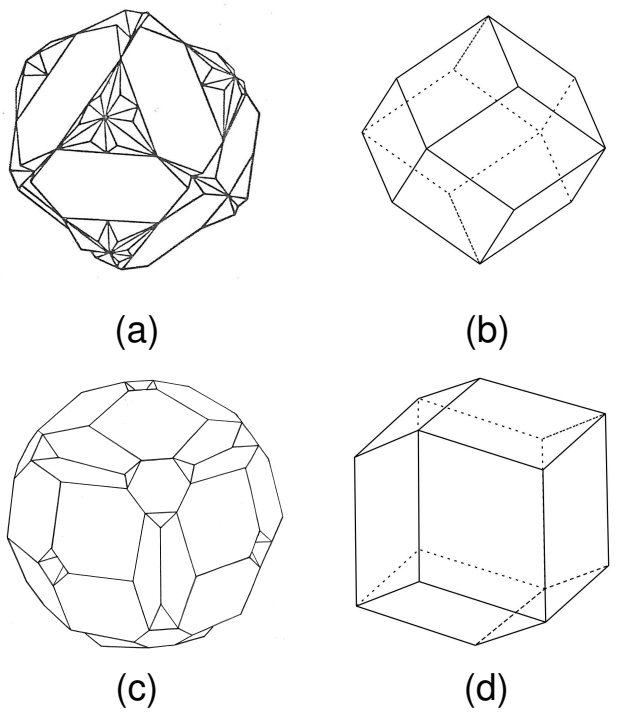

FIG. 7. (a) Fourth Brillouin zone and (b) Jones zone of structures with FCC translational structure. (c) Fifth Brillouin zone of FCC structure and (d) Jones zone of the bismuth ($A7$) structure.

amond structure [Fig. 7(b)] is again much simpler than the fourth BZ [Fig. 7(a)] and has the same volume. The approach has been applied to other $\langle \mathbf{5} \rangle$ materials, including SnTe [75] [76]. The use of the NFE (or pseudopotential) model in extended **k**-space has been applied by Littlewood [24, and references therein] to many octet ($A^N B^{8-N}$) and ten-electron ($A^N B^{10-N}$) compounds. Nevertheless, the model of Jones has largely been ignored in the PCM and NGS fields, where structural changes are usually attributed to the 1D "Peierls distortion", where the mapping of a 3D problem onto one dimension requires simplifying assumptions about the interactions between p-orbitals [24, 77].

Mott and Jones [69, p. 167] focused on the lowering of the total energy: "When this is the case, the greater the energy gaps over the zone boundaries the lower will be the total energy .... In this way, then, we can see a simple reason for the relative displacement of the two face-centered lattices; it represents merely the tendency of the total energy to diminish as far as possible." The band structure calculations of As, Sb, and Bi by Cohen *et al.* [78] showed a valence band of predominantly p-bonding character separated from p-antibonding bands that are mostly unoccupied. Mixing of bonding and antibonding character and sp-hybridization occur, and the location of the few holes in the uppermost valence band and the few electrons in lowest conduction band are determined by these mixings. Both the internal displacement and the trigonal shear are needed to explain the semimetallic behavior. It was confirmed much later that the former led to a very narrow gap semiconductor, and the latter drives a transition to a semimetal by a mechanism "consistent with the Jones-Peierls model" [79]. The main features of the band structure are a hole pocket near T and an electron pocket near L, where both T and L are derived from the point L for FE bands for 10 electrons in the FCC unit cell (Fig. 5). The presence of two types of carrier means that the temperature dependence of the conductivity will be different from that in a metal. Conduction and valence band extremities in GeTe, SnTe, PbS, PbSe, and PbTe are also at or near L [80, 81].

C. Peierls distortions in disordered materials

Jones and Peierls described structural instabilities using arguments based on the NFE theory of electronic structure in a crystal, but disordered systems show related features and are important in the context of crystallization. Tight-binding calculations in real space for systems containing elements of groups 15, 16, and 17 [82] show changes in coordination numbers and the presence of alternating short and long bonds that indicate that Peierls distortions occur in liquid P and As. Density functional/molecular dynamics (DF/MD) simulations of ℓ-GeTe show a high level of alternating chemical order and provide evidence for a Peierls distortion just above the melting point [83] with a minimum in the electronic DOS near E_F.

Figure 8 shows the electronic DOS from density functional calculations in crystalline, amorphous, and liquid GST [84]. A small band gap (~ 0.2 eV) is present in the first two phases, and there is a minimum at E_F in the liquid. The measured band gaps at room temperature for c- and a-GST are 0.74 ± 0.5 eV and ~ 0.5 eV, respectively [85].

D. Crystallization: Ostwald's step rule

GST is a supercooled liquid at 600 K, and the history of metastable structure formation in liquids goes back to the 19th century and the work of Ostwald [86], who summarized his observations of crystallization with his *Stufensatz* ('step rule' or 'rule of stages'): for a metastable (or unstable) liquid that can crystallize in several forms, the first stage of nucleation is to the metastable form nearest in free energy, not to the most stable form. The ordering of free energies could be determined by considering phases of variable concentration or structure. A refinement by Stranski and Totomanow [87] focused on the metastable form that is separated from the initial state by the lowest free energy barrier. This opens the prospect of finding alternative multistep paths to the most stable form involving a variety of structures (polymorphs), and

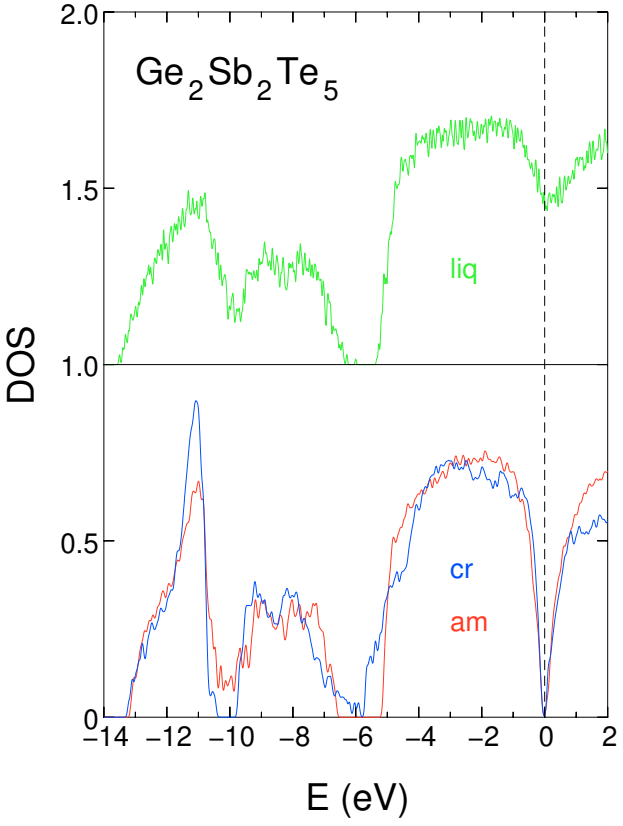

FIG. 8. Calculated electronic density of states of amorphous (am, red), crystalline (cr, blue), and liquid GST at 900 K (liq, green) [84]. The vertical dashed line at $E = 0$ marks the Fermi energy. Amorphous and crystalline calculations used a 2×2×2 Monkhorst-Pack mesh, the liquid DOS is based on five snapshots with one k-point ($k = 0$).

various models have been used to study crystallization in the presence of multiple metastable intermediate phases [88, and references therein].

Ostwald's step rule and the Stranski-Totomanov extension often hold, but well-documented counterexamples [89, 90] show that neither is rigorous, and this was clear already to Ostwald. However, van Santen [91] applied irreversible thermodynamics to show that a multiple step reaction leads to a lower entropy production than the direct reaction, and simulations of ten Wolde and Frenkel [92] showed that pathways for homogeneous nucleation could differ markedly from classical nucleation theory and follow a *microscopic* version of Ostwald's rule. The presence of a metastable liquid-liquid critical point lowers the free energy barrier and increases the nucleation rate during the crystallization of biological molecules [93] and multicomponent systems [94]. Femtosecond x-ray diffraction studies of the PCM AIST and $Ge_{15}Sb_{85}$ show the presence of liquid-liquid phase transitions [95].

IV. CRYSTALLIZATION IN GST

We now summarize the structural changes taking place during crystallization of a-GST and show that they can be rationalized using a model based on the above.

A. Results of simulations and experiment

Density functional simulations [84, 96, 97] of amorphous and liquid (ℓ)-GeTe and GST show the presence of vacancies and $ABAB$-rings (A: Ge, Sb, B: Te) in all phases. In a-GST, the distributions of Te-Sb-Te and Te-Ge-Te bond angles show pronounced peaks around 90°, and the dihedral angles for Ge-Te and Sb-Te bonds show maxima around 0, 90°, and 180° that also arise in cubic structures. Simulations of crystallization of a-GST [26–29] showed that $ABAB$ rings reorient on a nanosecond time scale to the metastable RS structure [15] with Te atoms on the anion sublattice and an apparently disordered arrangement of Ge, Sb, and vacancies on the cation sublattice. The vibration frequencies of GST (typically 3 THz [84]) allow several thousand vibrations on the scale of nanoseconds, and energy minimization leads to a substantial rearrangement of the $ABAB$ rings and a dramatic reduction in the number of "wrong bonds" (Ge-Ge, Ge-Sb, Sb-Sb, Te-Te). The ordering of Te atoms in the cation sublattice is rapid, but slower ordering of the other elements and vacancies occurs. The overall picture is motion of Ge and Sb atoms away from vacancies, which accumulate in the neighborhood of Te atoms. The distribution of vacancies around Te atoms found in the simulations agrees well with the results of ^{125}Te nuclear magnetic resonance studies [98].

Fig. 9 shows a snapshot of the ordered structure of GST in [27]. The atoms in the anion lattice show clear signs of segregation, so that their distribution is definitely not random. The time dependence of the associated partial pair distribution functions and coordination numbers confirm this ([27], including Supplementary Information, [28]). STEM measurements and DF calculations [99] show that further annealing results in vacancy segregation into specific (111) planes of the trigonal structure discussed above.

B. Model

The main driving force for structural changes in GST is the energy lowering accompanying the occupation of bonding orbitals, and the number of vacancies in the metastable RS phases of the PCM $(GeTe)_{1-x}(Sb_2Te_3)_x$ is such that that all bonding p-orbitals are occupied [58]. It is common to associate p^3-configurations with cubic structures, and an SC structure, viewed as two FCC lattices displaced along the cubic diagonal (Fig. 6), is unstable against a combined trigonal shear and rhombohedral distortion. This occurs in the elements As, Sb, and Bi,

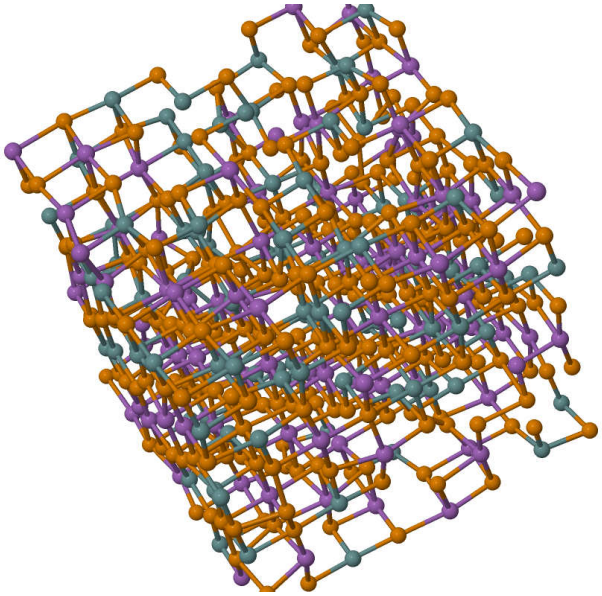

FIG. 9. Structure of (metastable) crystalline GST [28]. Orange: Te, grey: Ge, purple: Sb. Ordering in the Te layers is almost complete. Segregation in the other layers is evident.

and GeTe is rhombohedral at room temperature and has an RS structure at high temperatures. These materials have exactly five valence electrons (s^2p^3) per atom, and Jones [68] explained the structure and semimetallic properties of Bi using a nearly free electron (NFE) model in the extended zone scheme with 10 electrons (five per atom) filling a zone constructed in **k**-space. The number of valence electrons in the pseudobinary PCM mentioned above is close to five (4.75 in $Ge_1Sb_4Te_7$, x=2/3; 4.91 in $Ge_8Sb_2Te_{11}$, x=1/9).

The s- and p-valence orbitals in Ge, Sb, and Te atoms are very similar, and the principle of maximum overlapping implies that the energy lowering in GST will be greater than in other combinations of atoms of the same groups. The similarity is a direct consequence of "secondary periodicity," where the "d-block contraction" of the valence orbitals of Ge balances the orbital contraction found in Sb (group 15) and Te (group 16) to the right of Ge in the periodic table.

These observations allow us to consider a model for the crystallization of amorphous GST, where the structure has many cubic features. If we focus on the cubic aspects alone, assume that the orbitals of Ge, Sb, and Te are the *same*, not just similar, and that the GST systems have an *average* of five valence electrons (s^2p^3) per site, including vacancies, we can adapt the arguments applied to Bi by Jones [68] to rationalize the rock salt metastable structures found in both experiments and simulations of Ge/Sb/Te alloys. The structural changes must also reflect the composition of the material and the different electronic configurations and valences of the components, Ge $3s^23p^2$, Sb $4s^24p^3$, Te $4s^24p^4$, and vacancies s^0p^0. The most stable average configuration (s^2p^3) can be maintained if Sb and particularly Ge atoms move away from vacancies, which accumulate near Te atoms. These trends are observed in the simulations, where the lighter Ge atoms are also more mobile than Sb, and very few vacancies have Ge or Sb atoms as neighbors in the ordered metastable structure [27]. Te atoms make up at least half of the total number in all Ge/Sb/Te alloys near the tie-line, and attainment of an average configuration of s^2p^3 with these constraints will favor a Te sublattice.

The formation of a metastable state well above the energy of the most stable (trigonal) structure is an example of Ostwald's step rule in a multicomponent system. The free energy is lowered by the distortion to the metastable RS structure with the most rapid kinetics. The accompanying process to the most stable structure is much slower, but the first stages of order—the segregation of Ge and Sb atoms—are evident in DF/MD simulations. It will be interesting to see whether the lack of randomness can be confirmed experimentally.

V. DISCUSSION AND CONCLUDING REMARKS

The requirements of PCM are satisfied to varying extents by many compounds of elements of groups 14, 15, and 16, but almost all commercial products use alloys containing Ge, Sb, and/or Te. The time-limiting step in the read-write cycle is crystallization of amorphous bits, which is driven by the lowering of energy on bond formation. This is greatest when the overlap of the valence orbitals is maximized, and this occurs in Ge, Sb, and Te (see Sec. II C); Sb and Te are adjacent in the periodic table, and the d-block contraction in Ge counteracts the expansion usually associated with elements in a column to the left. Structural consequences of "secondary periodicity" are evident in the chalcogenides of Ge: GeTe is rhombohedral, while GeS and GeSe are orthorhombic [39], and GeTe crystallizes much more readily than GeSe and $GeSe_2$ [3].

Unlike the distance where a valence orbital has its maximum value, radial moments (Fig. 2, Table I) contain information over the whole range and are used here to characterize the orbitals. Choosing elements with comparable radial moments results in materials with weak sp-hybridization and small charge transfer between the atoms. Secondary periodicity is also evident in eigenvalue plots (Fig. SF4), but variations with Z are less pronounced than in the orbital moments (Fig. 2), which also provide a guide to finding alternatives to Ge, Sb, and Te as PCM.

A good match to Ge is provided by Si, but the sp-splitting is smaller in Si and hybridization more pronounced. Se and As, like Ge, are subject to the d-block contraction, and the overlap of their orbitals with those of Ge is less than for Te and Sb, respectively. The short half-life of all isotopes eliminates Po as a replacement

for Te, and Bi shares with Po and other elements with $Z > 80$ a pronounced relativistic contraction of the *s*-orbital, weak *sp*-hybridization, and a tendency to favor cubic over rhombohedral structures. The replacement of a fraction of Sb by Bi or Ge by Sn may still be favorable. The instability towards crystallization of pure amorphous Te and Sb means that additional components are essential. One suggestion was to develop multielement substances with atoms of different sizes and chemical bonding states, noting that "GST, AIST, and GeST are all multielement substances in which Sb and Te (which have large atomic radii) and Ge, Ag, and In (which have small atomic radii) are mixed together" [4]. The orbital functions of Ag and In in AIST are, however, significantly *more* extended than those of Sb and Te (Fig. SF6). This means that the present analysis would require modification for the compounds of In with Ge, Sb, and/or Te mentioned above.

There have been numerous attempts to rationalize the behavior of PCM and other narrow gap semiconductors comprising elements near the diagonal of the periodic table between B and Po. Pauling and others refer to these elements as *metalloids*, which have "... properties intermediate between those of metals and those of nonmetals" [100, p. 612], and Littlewood noted: "To understand the structural properties of narrow gap semiconductors, it is necessary to consider them as borderline cases in the broad trend from covalent to metallic binding" [24, p. 232].

It has been proposed that the function of PCM reflects drastic changes in the nature of the chemical bond in the two phases: "resonant bonding" in the crystal [101], transient three-center bonds mediated by lone pair electrons [102], or "metavalent bonding" in "incipient metals" [103]. Alignment of *p*-orbitals in the ordered structure has been invoked as a requirement for large optical contrast in PCM [104]. The identification of particular bonding mechanisms is not always straightforward; any molecular orbital ("delocalized") function can be transformed into a valence bond ("localized") function [31, and references therein], and a wave function can be projected in a variety of ways to give atomic, ionic, or other components [105].

We have focused here on the relationship between the structure and the *number* of valence electrons of the component atoms, the extent of their orbitals as characterized by the radial moments, and the NFE model of band theory in the extended zone scheme, as well as the composition of the materials. All aspects are important, so that the focus is broader than requiring an average count of 3 *p*-electrons per site [25, 58]. The "band" (reciprocal space) and "bond" (real space) perspectives provide complementary information about structure and bonding. In the context of $\langle \mathbf{5} \rangle$ materials, Cohen *et al.* concluded that the "band" picture provided a "deeper basis for understanding" [78], and the electronic structure has been emphasized here. The NFE approach is the basis of the structural distortion models developed by Jones and by Peierls, and it is close to the density functional formalism [43] used in most simulations of PCM. It shows that dramatic changes in electronic and structural properties can result without invoking different bonding mechanisms. In the case of bulk Al and Si, for example, the different number of valence electrons leads to the difference between an FCC metal and a semiconductor with a diamond structure and a gap of over 1 eV. Large changes can occur in Ge/Sb/Te materials as well. The actual *mechanism* of bonding in these materials in their different phases is a lowering of kinetic energy due to wave function overlap [43, 106] with only differences in detail.

ACKNOWLEDGMENTS

I thank J. Akola and J. Kalikka for discussions and collaboration on GST simulations, B. J. Kooi and H. R. Schober for helpful comments, and O. Khomenko for translating parts of [47]. Computer time provided by the JARA-HPC Vergabegremium on the JARA-HPC partition of the supercomputers JUQUEEN and Jureca (Forschungszentrum Jülich) is acknowledged gratefully.

[1] S. R. Ovshinsky, Phys. Rev. Lett. **21**, 1450 (1968).
[2] M. Takenaga, N. Yamada, S. Ohara, K. Nishiuchi, M. Nagashima, T. Kashihara, S. Nakamura, and T. Yamashita, Proc. SPIE Int. Soc. Opt. Eng. **420**, 173 (1983).
[3] M. Chen, K. A. Rubin, and R. W. Barton, Appl. Phys. Lett. **49**, 502 (1986).
[4] T. Matsunaga and N. Yamada, Jpn. J. Appl. Phys. **43**, 4704 (2004).
[5] N. K. Abrikosov and G. T. Danilova-Dobryakova, Izv. Akad. Nauk USSR, Neorg. Mater. **1**, 204 (1965).
[6] N. K. Abrikosov and G. T. Danilova-Dobryakova, Izv. Akad. Nauk USSR, Neorg. Mater. **1**, 57 (1965).
[7] L. E. Shelimova, O. G. Karpinskii, M. A. Kretova, V. I. Kosyakov, V. A. Shestakov, V. S. Zemskov, and F. A. Kuznetsov, Inorg. Mater. **36**, 768 (2000).
[8] E. Spreafico, S. Caravati, and M. Bernasconi, Phys. Rev. B **83**, 144205 (2011).
[9] V. L. Deringer, W. Zhang, P. Rausch, R. Mazzarello, R. Dronskowski, and M. Wuttig, J. Mater. Chem. C **3**, 9519 (2015).
[10] S. Gabardi, S. Caravati, J. H. Los, T. D. Kühne, and M. Bernasconi, J. Chem. Phys. **144**, 204508 (2016).
[11] S. Gabardi, D. Campi, and M. Bernasconi, J. Comput. Electron. **16**, 1003 (2017).
[12] N. Yamada, E. Ohno, N. Akahira, K. Nishiuchi, K. Nagata, and M. Takao, Jpn. J. Appl. Phys. **26**, 61 (1987).
[13] N. Yamada, E. Ohno, K. Nishiuchi, N. Akahira, and M. Takao, J. Appl. Phys. **69**, 2849 (1991).
[14] N. Yamada, Phys. Status Solidi B **249**, 1837 (2012).

[15] N. Yamada, MRS Bulletin **21**, 48 (1996).
[16] T. Matsunaga, R. Kojima, N. Yamada, K. Kifune, Y. Kubota, Y. Tabata, and M. Takata, Inorg. Chem. **45**, 2235 (2006).
[17] B. J. Kooi and J. T. M. de Hosson, J. Appl. Phys. **92**, 3584 (2002).
[18] T. Matsunaga, N. Yamada, and Y. Kubota, Acta Cryst. B **60**, 685 (2004).
[19] A. M. Mio, S. M. S. Privitera, V. Bragaglia, F. Arciprete, C. Bongiorno, R. Calarco, and E. Rimini, Nanotechnology **28**, 065706 (2017).
[20] J. Akola and R. O. Jones, Phys. Rev. B **79**, 134118 (2009).
[21] J. Momand, R. Wang, J. E. Boschker, M. A. Verheijen, R. Calarco, and B. J. Kooi, Nanoscale **9**, 8774 (2017).
[22] F. Rao, K. Ding, Y. Zhou, Y. Zheng, M. Xia, S. Lv, Z. Song, S. Feng, I. Ronneberger, R. Mazzarello, W. Zhang, and E. Ma, Science **358**, 1423 (2017); J. Akola and R. O. Jones, *ibid.* **358**, 1386 (2017).
[23] M. Salinga, B. Kersting, I. Ronneberger, V. P. Jonnalagadda, X. T. Vu, M. Le Gallo, I. Giannopoulos, O. Cojocaru-Mirédin, R. Mazzarello, and A. Sebastian, Nat. Mater. **17**, 681 (2018).
[24] P. B. Littlewood, CRC Crit. Rev. Solid State Mater. Sci. **11**, 229 (1983).
[25] D. Lencer, M. Salinga, B. Grabowski, T. Hickel, J. Neugebauer, and M. Wuttig, Nat. Mater. **7**, 972 (2008).
[26] J. Kalikka, J. Akola, J. Larrucea, and R. O. Jones, Phys. Rev. B **86**, 144113 (2012).
[27] J. Kalikka, J. Akola, and R. O. Jones, Phys. Rev. B **90**, 184109 (2014).
[28] J. Kalikka, J. Akola, and R. O. Jones, Phys. Rev. B **94**, 134105 (2016).
[29] I. Ronneberger, W. Zhang, H. Eshet, and R. Mazzarello, Adv. Funct. Mater. **25**, 6407 (2015).
[30] F. C. Mocanu, K. Konstantinou, T. H. Lee, N. Bernstein, V. L. Deringer, G. Csányi, and S. R. Elliott, J. Phys. Chem. B **122**, 8998 (2018).
[31] R. O. Jones, J. Phys.: Condens. Matter **30**, 153001 (2018).
[32] L. Pauling, *The Nature of the Chemical Bond*, 3rd ed. (Cornell University Press, Ithaca, N.Y., 1960) Chap. 3.
[33] R. S. Mulliken, J. Chem. Phys. **2**, 782 (1934).
[34] J. C. Phillips and J. A. van Vechten, Phys. Rev. B **2**, 2147 (1970).
[35] J. St. John and A. N. Bloch, Phys. Rev. Lett. **33**, 1095 (1974).
[36] D. Schiferl, Phys. Rev. B **10**, 3316 (1974).
[37] J. K. Burdett, G. D. Price, and S. L. Price, Phys. Rev. B **24**, 2903 (1981).
[38] A. Zunger and M. L. Cohen, Phys. Rev. B **20**, 4082 (1979).
[39] P. B. Littlewood, J. Phys. C: Solid State Phys. **13**, 4855 (1980).
[40] J.-Y. Raty, M. Schumacher, P. Golub, V. L. Deringer, C. Gatti, and M. Wuttig, Adv. Mater. **31**, 1806280 (2019).
[41] J. C. Slater, Phys. Rev. **37**, 481 (1931).
[42] L. Pauling, J. Am. Chem. Soc. **53**, 1367 (1931).
[43] R. O. Jones, Rev. Mod. Phys. **87**, 897 (2015).
[44] J. P. Perdew, K. Burke, and M. Ernzerhof, Phys. Rev. Lett. **77**, 3865 (1996).
[45] D. R. Hamann, Phys. Rev. B **40**, 2980 (1989).
[46] J. H. Wood and A. M. Boring, Phys. Rev. B **18**, 2701 (1978), . The large component radial orbital is solved explicitly in the self-consistent cycle, and the small component is determined from it by perturbation theory.
[47] E. V. Biron, Zh. Russ. Fiz.-Khim. Obshch. **47**, 964 (1915).
[48] S. A. Shchukarev, J. Gen. Chem. USSR **25**, 595 (1954).
[49] R. S. Nyholm, Proc. Chem. Soc. **1961**, 273 (1961).
[50] P. Pyykkö, Chem. Rev. **88**, 563 (1988), and references therein.
[51] V. M. Goldschmidt, T. Barth, and G. Kunde, Norsk. Vid. Akad. Skr. 1, M.-N. Kl. **7**, 1 (1925).
[52] Plots of valence s- and p-orbitals of atoms of groups 13, 15, and 16 are provided as Supplementary Material at http://doi.org/10.yyyy/xxxx.
[53] The maxima of $R_{nl}(r)$ for $l = 0, 1$ are at the following radii (Å): Ge (0.93,1.17), Sb (1.00,1.24), Te (0.94,1.15).
[54] R. O. Jones, J. Chem. Phys. **99**, 1194 (1993).
[55] J. Harris and R. O. Jones, Phys. Rev. A **19**, 1813 (1979).
[56] See `https://en.wikipedia.org/wiki/Electronegativity` retrieved on 23 June 2019.
[57] J. Robertson, K. Xiong, and P. Peacock, Thin Solid Films **515**, 7538 (2007).
[58] M. Luo and M. Wuttig, Adv. Mater. **16**, 439 (2004).
[59] J. Donohue, *The Structures of the Elements* (Wiley, New York, 1974) Chap. 8.
[60] R. O. Jones and D. Hohl, J. Chem. Phys. **92**, 6710 (1990).
[61] P. Ballone and R. O. Jones, J. Chem. Phys. **100**, 4941 (1994).
[62] R. O. Jones, O. Ahlstedt, J. Akola, and M. Ropo, J. Chem. Phys. **146**, 194502 (2017).
[63] The structure of α-Sb is a small rhombohedral perturbation on a simple cubic (SC) structure [59, p. 307], but a wedge-shaped (C_{2v}) structure of Sb_8 (bond angles from 60–110°) is almost 0.7 eV more stable than the cubic (O_h) form [62]. Similar C_{2v} structures arise in P_n clusters [60] and monoclinic P [59, p. 294].
[64] R. Peierls, Ann. Phys.-Berlin **396**, 121 (1930).
[65] F. Bloch, Z. Physik **52**, 555 (1929).
[66] L. Brillouin, J. Phys. Radium **1**, 377 (1930).
[67] J. M. Ziman, *Electrons and Phonons. The Theory of Transport Phenomena in Solids* (Clarendon Press, Oxford, 1960) Chap. 2.
[68] H. Jones, P. R. Soc. A **147**, 396 (1934).
[69] N. F. Mott and H. Jones, *The Theory of the Properties of Metals and Alloys* (Clarendon Press, Oxford, 1936).
[70] R. E. Peierls, *Quantum Theory of Solids* (Clarendon Press, Oxford, 1955).
[71] H. Jones, *The Theory of Brillouin Zones and Electronic States in Crystals*, second, revised ed. (North-Holland, Amsterdam, 1975).
[72] SC: u=0.250, α=60°; Bi: 0.237, 57.27°; Sb: 0.233, 56.60°; As: 0.226, 54.12° [69, p. 167].
[73] S_{221} is zero in the SC structure, but is large for small trigonal displacements in As, Sb, and Bi.
[74] V. Heine and R. O. Jones, J. Phys. C: Solid St. Phys. **2**, 719 (1969).
[75] Y. Onodera, Solid State Commun. **11**, 1397 (1972).
[76] Onodera [75] and Littlewood [24] refer to the "Jones zone" of the group 14-16 materials, but both show the fifth BZ of the FCC structure [Fig. 7(c)].
[77] J.-P. Gaspard and R. Ceolin, Solid State Commun. **84**, 839 (1992).

[78] M. H. Cohen, L. M. Falicov, and S. Golin, IBM Journal **8**, 215 (1964).
[79] A. B. Shick, J. B. Ketterson, D. L. Novikov, and A. J. Freeman, Phys. Rev. B **60**, 15484 (1999).
[80] F. Herman, R. L. Kortum, I. B. Ortenburger, and J. P. Van Dyke, J. Phys. Colloques **29**, 62 (1968).
[81] H. M. Polatoglou, G. Theodorou, and N. A. Economou, in *Physics of Narrow Gap Semiconductors*, edited by E. Gornik, H. Heinrich, and L. Palmetshofer (Springer, Berlin, Heidelberg, 1982) pp. 221–225.
[82] J.-P. Gaspard, C. R. Physique **17**, 389 (2016), and references therein.
[83] J. Y. Raty, V. Godlevsky, P. Ghosez, C. Bichara, J. P. Gaspard, and J. R. Chelikowsky, Phys. Rev. Lett. **85**, 1950 (2000).
[84] J. Akola and R. O. Jones, J. Phys.: Condens. Matter **20**, 465103 (2008).
[85] T. Kato and K. Tanaka, Jpn. J. Appl. Phys. **44**, 7340 (2005).
[86] W. Ostwald, Z. Phys. Chem. **22**, 289 (1897).
[87] I. N. Stranski and D. Totomanow, Z. Phys. Chem. **163**, 399 (1933).
[88] M. Santra, R. S. Singh, and B. Bagchi, J. Phys. Chem. B **117**, 13154 (2013).
[89] T. Threlfall, Org. Process Res. Dev. **7**, 1017 (2003).
[90] L. O. Hedges and S. Whitelam, J. Chem. Phys. **135**, 164902 (2011).
[91] R. A. van Santen, J. Phys. Chem. **88**, 5768 (1984).
[92] P. R. ten Wolde and D. Frenkel, Phys. Chem. Chem. Phys. **1**, 2191 (1999).
[93] Y. Tahri, E. Gagnière, E. Chabanon, T. Bounahmidi, Z. Kožíšek, N. Candoni, S. Veesler, M. Boukerche, and D. Mangin, Cryst. Growth Des. **19**, 3329 (2019).
[94] P. Wen, P. Harrowell, and C. A. Angell, J. Phys. Chem. A **115**, 6260 (2011).
[95] P. Zalden, F. Quirin, M. Schumacher, J. Siegel, S. Wei, A. Koc, M. Nicoul, M. Trigo, P. Andreasson, H. Enquist, M. J. Shu, T. Pardini, M. Chollet, D. Zhu, H. Lemke, I. Ronneberger, J. Larsson, A. M. Lindenberg, H. E. Fischer, S. Hau-Riege, D. A. Reis, R. Mazzarello, M. Wuttig, and K. Sokolowski-Tinten, Science **364**, 1062 (2019).
[96] J. Akola and R. O. Jones, Phys. Rev. B **76**, 235201 (2007).
[97] J. Akola and R. O. Jones, Phys. Rev. Lett. **100**, 205502 (2008).
[98] S. Sen, T. G. Edwards, J.-Y. Cho, and Y.-C. Joo, Phys. Rev. Lett. **108**, 195506 (2012).
[99] B. Zhang, W. Zhang, Z. Shen, Y. Chen, J. Li, S. Zhang, Z. Zhang, M. Wuttig, R. Mazzarello, E. Ma, and X. Han, Appl. Phys. Lett. **108**, 191902 (2016).
[100] L. Pauling, *General Chemistry*, 3rd ed. (Freeman, San Francisco, 1970).
[101] K. Shportko, S. Kremers, M. Woda, D. Lencer, J. Robertson, and M. Wuttig, Nat. Mater. **7**, 653 (2008).
[102] A. Kolobov, P. Fons, and J. Tominaga, Sci. Rep. **5**, 13698 (2015).
[103] M. Wuttig, V. L. Deringer, X. Gonze, C. Bichara, and J.-Y. Raty, Adv. Mater. **30**, 1803777 (2018).
[104] B. Huang and J. Robertson, Phys. Rev. B **81**, 081204 (2010).
[105] S. Mukhopadhyay, J. Sun, A. Subedi, T. Siegrist, and D. J. Singh, Sci. Rep. **6**, 25981 (2016).
[106] K. Ruedenberg, Rev. Mod. Phys. **34**, 326 (1962).